

Generic Fe buffer layers for Fe-based superconductors: Epitaxial $\text{FeSe}_{1-x}\text{Te}_x$ thin films

Kazumasa Iida,^{1, a)} Jens Hanisch,¹ Michael Schulze,² Saicharan Aswartham,² Sabine Wurmehl,² Bernd Buchner,² Ludwig Schultz,¹ and Bernhard Holzapfel¹

¹⁾ *Institute for Metallic Materials, IFW Dresden, D-01171 Dresden, Germany*

²⁾ *Institute for Solid State Research, IFW Dresden, D-01171 Dresden, Germany*

(Dated: 18 November 2011)

Biaxially textured $\text{FeSe}_{1-x}\text{Te}_x$ films have been realized on Fe-buffered MgO substrates by pulsed laser deposition. Similar to the Fe/BaFe₂As₂ bilayers, the crystalline quality of $\text{FeSe}_{1-x}\text{Te}_x$ films exhibit a sharp out-of-plane and in-plane texture less than 0.9°. The Fe/ $\text{FeSe}_{1-x}\text{Te}_x$ bilayers showed high superconducting transition temperatures of over 17 K. The angular-dependent critical current densities exhibit peaks positioned at $H \perp c$ similar to other pnictide thin films. The volume pinning force of $\text{FeSe}_{1-x}\text{Te}_x$ in this direction is very strong compared with that of Co-doped BaFe₂As₂, due to a good matching between the interlayer distance in the c direction and the out-of-plane coherence length.

PACS numbers: 74.70.Xa, 81.15.Fg, 74.78.-w, 74.25.Sv, 74.25.F-

Epitaxial iron chalcogenide superconducting thin films have been prepared on single crystalline oxides substrates by pulsed laser deposition (PLD) or molecular beam epitaxy (MBE) to investigate their intrinsic properties and to explore superconducting device applications.^{1–6} These superconductors are very sensitive to strain.⁵ Indeed, the superconducting transition temperature (T_c) of $\text{FeSe}_{0.5}\text{Te}_{0.5}$ films can be tuned by strain and even higher T_c values in films than in bulk materials can be realized.⁷ In addition, the superconductivity is induced in FeTe films by the tensile stress albeit their bulk crystals are not superconducting at ambient pressure.⁸

The biaxial strain is usually induced by a lattice mismatch between films and substrates. However, the correlation between T_c and lattice mismatch for $\text{FeSe}_{0.5}\text{Te}_{0.5}$ is controversial.⁹ A fundamental problem is the formation of an interfacial layer between $\text{FeSe}_{0.5}\text{Te}_{0.5}$ and oxide substrates,⁹ which compromises the epitaxial growth. Later the interfacial layer was identified as amorphous containing oxygen, which comes mainly from oxide substrates.¹⁰ Furthermore, oxygen diffusion into the films was detected by transmission electron microscope (TEM) analyses, which deteriorates the superconducting properties. In order to minimize the oxygen diffusion, Tsukada *et al.* have proposed the implementation of CaF₂ substrates, resulting in good superconducting properties.¹¹ Hence, ideal growth conditions of $\text{FeSe}_{1-x}\text{Te}_x$ thin films require non-oxide substrates under ultra-high vacuum (UHV) atmosphere.

Recently we have reported that epitaxial Co-doped BaFe₂As₂ (Ba-122) films can be realized on Fe-buffered single crystalline MgO substrates in UHV condition.¹² The detailed TEM analyses revealed that the FeAs tetrahedron in the Ba-122 bonds coherently to body centered cubic Fe. This Fe/Ba-122 bilayer has a clean mi-

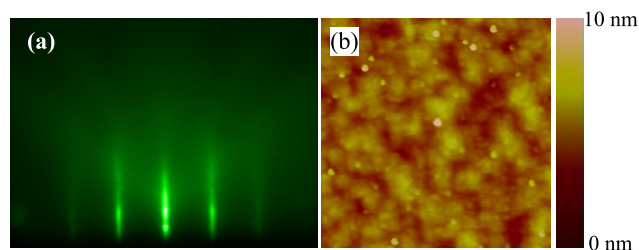


FIG. 1. (Color online) (a) The RHEED image of $\text{FeSe}_{1-x}\text{Te}_x$ at room temperature shows only streaks, indicative of a flat surface. The incident electron beam is the MgO [110] azimuth. (b) The corresponding AFM image ($1\mu\text{m} \times 1\mu\text{m}$) shows an R_{rms} value of 0.73 nm.

crostructure and is of excellent crystalline quality without grain boundaries (GBs).¹³ Since the FeAs or FeSe(Te) tetrahedron is a common structure for both Ba-122 and $\text{FeSe}_{1-x}\text{Te}_x$, the implementation of an Fe buffer should be also applicable for the epitaxial growth of $\text{FeSe}_{1-x}\text{Te}_x$. In this letter, we demonstrate the implementation of an Fe buffer layer to grow epitaxial $\text{FeSe}_{1-x}\text{Te}_x$ films and present their transport properties.

The Fe/ $\text{FeSe}_{1-x}\text{Te}_x$ bilayers were prepared by PLD (KrF excimer laser, $\lambda = 248\text{ nm}$), which is almost identical deposition methods to Fe/Ba-122 except for the deposition temperature and the laser repetition rate of $\text{FeSe}_{1-x}\text{Te}_x$. The energy density of the laser on the target was 3–5 J/cm² and the distance between target and substrate was approximately 6 cm. Single crystalline MgO (100) substrates were heated to 1000 °C, held at this temperature for 30 min, and subsequently cooled to room temperature for cleaning. After the Fe deposition at room temperature, the Fe-covered MgO was heated to 750 °C, held at this temperature for 20 min and subsequently cooled to 450 °C, the optimum deposition temperature of $\text{FeSe}_{1-x}\text{Te}_x$ films with highest T_c value, similarly to the results in Ref.³. Once the temperature

^{a)} Electronical address: k.iida@ifw-dresden.de

was stabilized, the $\text{FeSe}_{1-x}\text{Te}_x$ layer was deposited at a laser frequency of 3 Hz. The whole deposition process was conducted under UHV condition (base pressure of 10^{-10} mbar). The respective layer thickness of Fe and $\text{FeSe}_{1-x}\text{Te}_x$ were 20 nm and 95 nm confirmed by cross-sectional focused ion beam cuts at different sample areas as well as TEM.

The PLD target was prepared by a modified Bridgman technique yielding an Fe-Te-Se crystal with the nominal composition of $\text{Fe}:\text{Se}:\text{Te}=1:0.5:0.5$. For the growth, stoichiometric amounts of pre-purified metals were sealed in an evacuated quartz tube. The tube was placed in a horizontal tube furnace and heated up to 650°C and kept at that temperature for 24 h. The furnace was then heated to 950°C and the temperature was kept constant for 48 h. Finally, the furnace was cooled down with a rate of $5^\circ\text{C}/\text{h}$ to 770°C , followed by furnace cooling. We yield crystals with dimensions up to cm-size. A bulk T_c of 13.6 K was recorded by a superconducting quantum interface device (SQUID) magnetometer. Details of the single crystal preparation and their properties can be found in Ref.¹⁴.

Each deposition step was monitored by reflection high-energy electron diffraction (RHEED). The RHEED image of the $\text{FeSe}_{1-x}\text{Te}_x$ acquired at room temperature, fig.1(a), shows only streaks similarly to the Fe buffer layer. This is indicative of a smooth surface of the $\text{FeSe}_{1-x}\text{Te}_x$ layer, which is consistent with the observation by atomic force microscope (AFM) presented in fig.1(b). A root mean square roughness (R_{rms}) of 0.73 nm was recorded.

In order to check phase purity and texture quality of the films, detailed structural characterizations by x-ray diffraction were conducted as summarized in fig. 2. The $\theta/2\theta$ -scans, fig. 2(a), show only $00l$ reflections of $\text{FeSe}_{1-x}\text{Te}_x$ together with the 002 reflection of Fe and MgO, indicating c -axis texture and phase purity. The ω -scan for the 001 reflection of $\text{FeSe}_{1-x}\text{Te}_x$ in fig. 2(b) shows a sharp full width at half maximum (FWHM, $\Delta\omega$) of 0.72° . The 101 pole figure measurements and the corresponding ϕ -scans of $\text{FeSe}_{1-x}\text{Te}_x$ reveal no satellite and additional reflections other than sharp and strong reflections at every 90° , indicative of biaxial texture. Here, the epitaxial relation is identified as $(001)[100]\text{FeSe}_{1-x}\text{Te}_x \parallel (001)[110]\text{Fe} \parallel (001)[100]\text{MgO}$. The average $\Delta\phi$ of Fe and $\text{FeSe}_{1-x}\text{Te}_x$ are 1.05° and 0.83° , respectively. From these results, the $\text{FeSe}_{1-x}\text{Te}_x$ layer is of good crystalline quality without GBs.

In order to avoid any damage during ion beam etching and to ensure a low contact resistance, an Au layer was deposited on the film at room temperature by PLD. The Au-covered $\text{FeSe}_{1-x}\text{Te}_x$ film was then ion beam etched to form bridges with 0.5 mm width and 1 mm length for transport measurements, which were conducted in a Physical Property Measurement System (PPMS, Quantum Design) by a four-probe method. Here, a criterion of $1 \mu\text{Vcm}^{-1}$ (E_c) was used for evaluating J_c .

The $\text{FeSe}_{1-x}\text{Te}_x$ film exhibits no sign of a resistance

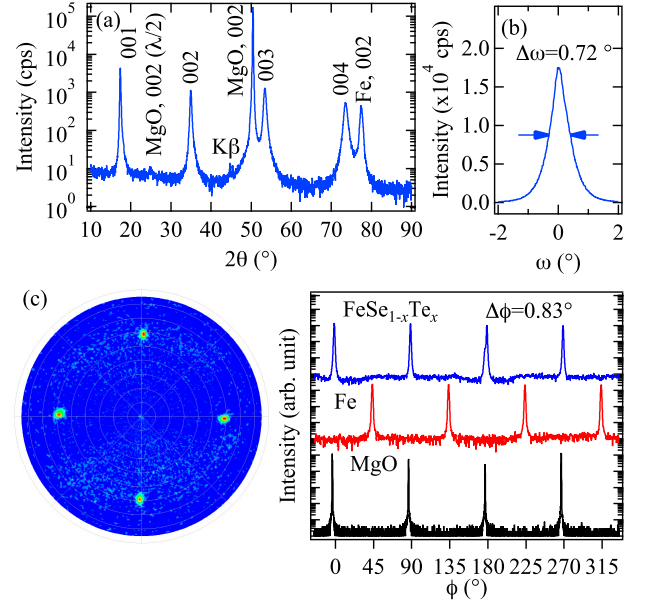


FIG. 2. (Color online) (a) The $\theta/2\theta$ -scan of an $\text{FeSe}_{1-x}\text{Te}_x$ bilayer in Bragg-Brentano geometry using $\text{Co-K}\alpha$ radiation. Both layers of Fe and $\text{FeSe}_{1-x}\text{Te}_x$ were grown with c -axis texture. (b) Rocking curve of the 001 reflection. $\Delta\omega = 0.72^\circ$ indicates good out-of-plane texture. (c) The 101 pole figure measurement and the corresponding ϕ -scans of $\text{FeSe}_{1-x}\text{Te}_x$. The respective ϕ -scans of the 110 Fe and the 220 MgO are also presented. The average $\Delta\phi$ of Fe and $\text{FeSe}_{1-x}\text{Te}_x$ are 1.05° and 0.83° , respectively.

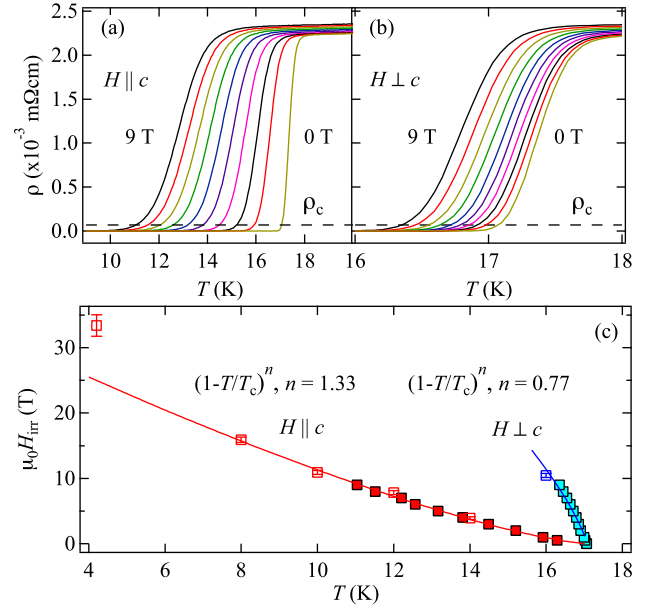


FIG. 3. (Color online) (a) Resistivity traces for $\text{FeSe}_{1-x}\text{Te}_x$ film measured in several magnetic fields for $H \parallel c$ and (b) $H \perp c$. Field increment is 1 T. Broken lines indicate the ρ_c for $\mu_0 H_{\text{irr}}$. (c) $\mu_0 H_{\text{irr}}$ for $H \parallel c$ are always lower than that for $H \perp c$. Open symbols are evaluated by the Kramer extrapolation.

anomaly at around 200 K, which has been frequently observed in $\text{FeSe}_{1-x}\text{Te}_x$ thin films. In addition, relatively small resistivity and a high residual resistivity ratio of 3.5 is recorded. This is a consequence of the current shunting effect since the resultant film was fully covered with Au. Therefore, the normal state behavior is masked by Au. Nevertheless, the onset T_c is recorded at 17.7 K, which is higher than the bulk value. The higher T_c might be due to the strain effect as reported in Ref.⁷. When magnetic fields are applied to the film, a clear shift of T_c to lower temperatures is observed for both directions, as exhibited in figs. 3(a) and (b). In particular, this shift together with a broadening of the transition is more significant for $H \parallel c$ than $H \perp c$. Figure 3(c) shows the temperature dependence of the irreversibility field (H_{irr}), which is defined by the intersection between the resistivity traces and the resistivity criterion (ρ_c) as shown in figs. 3(a) and (b). In addition, $\mu_0 H_{\text{irr}}$ evaluated by the Kramer extrapolation from $J_c - H$ characteristics presented later are also plotted.¹⁵ Here the ρ_c is defined as $E_c/J_{c,15}$, where the $J_{c,15} = 15 \text{ Acm}^{-2}$ is a criterion for H_{irr} in $J_c - H$ characteristics. In this definition, the N -value of the voltage-current characteristics ($V - I$, $V \propto I^N$) is 1 in the vicinity of E_c . It is clear from fig. 3(c) that $\mu_0 H_{\text{irr}}$ for $H \parallel c$ is always lower than that for $H \perp c$, indicating that the flux pinning is anisotropic. The $\mu_0 H_{\text{irr}}$ for $H \parallel c$ shows a power law relation, $\mu_0 H_{\text{irr}} \sim (1 - T/T_c)^n$, with exponent $n = 1.33 \pm 0.02$ in the temperature range from 8 K to 17 K. At 4.2 K, an increased value for $\mu_0 H_{\text{irr}}$ is observed presumably due to multi-band effects.¹⁶ On the other hand, an exponent of $n = (0.77 \pm 0.05) < 1$ is deduced for $H \perp c$, which is very similar to the upper critical field ($\mu_0 H_{c2}$) for $H \perp c$ in layered compounds (i.e. $\mu_0 H_{c2} \propto (1 - T/T_c)^{0.5}$).¹⁷

Shown in fig. 4(a) are $J_c - H$ characteristics measured for $H \parallel c$ at several temperatures. J_c values are quickly reducing with increasing H , indicative of less flux pinning in this direction. It should be noted that $V - I$ curves for evaluating J_c always show a power-law relation, suggesting that current is limited by depinning of flux rather than GBs. On the other hand, the reduction of J_c with H is very small for $H \perp c$ below 16 K (fig. 4(b)). The Se(Te)-Se(Te) interlayer distance in the c direction is almost identical to the out-of-plane coherence length at low temperatures ($\xi_c = 0.35 \text{ nm}$), resulting in strong pinning in this direction. Here the Se(Te)-Se(Te) interlayer distance is calculated as around 0.25 nm using $c(1 - 2z)$ with the lattice parameter c and the Se(Te) coordination z .⁵ For Co-doped Ba-122, the As-As interlayer distance in the c direction is 0.3 nm, which is far below ξ_c (1.2 nm). As a result, J_c at $H \perp c$ is decreased significantly with increasing H compared with $\text{FeSe}_{1-x}\text{Te}_x$. The volume pinning force (F_p) of $\text{FeSe}_{1-x}\text{Te}_x$ is larger than that of Co-doped Ba-122 for both major directions at reduced temperatures of $t = 0.68$ and 0.78 (fig. 4(c) and (d)). However, F_p of Co-doped Ba-122 for $H \parallel c$ is larger than that of $\text{FeSe}_{1-x}\text{Te}_x$ at $t = 0.48$ (not shown in this letter). The origin of this observation has to be investigated in detail

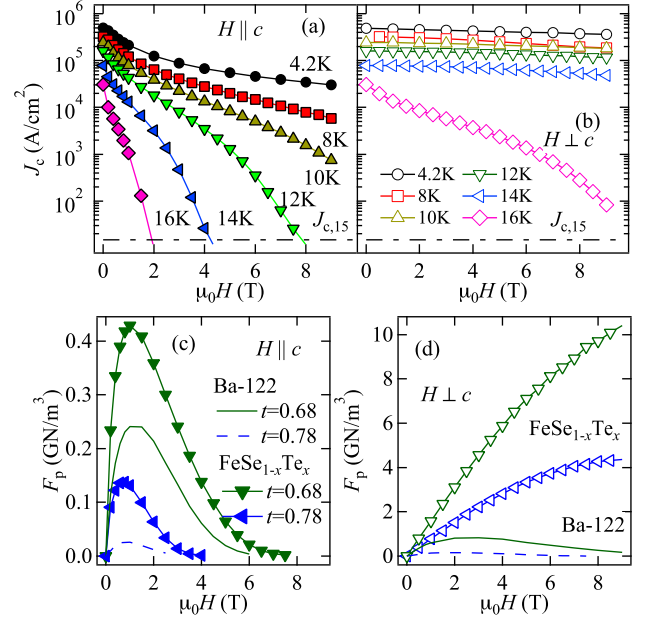


FIG. 4. (Color online) (a) $J_c - H$ characteristics measured in $H \parallel c$ and (b) $H \perp c$ at several temperatures. Chain lines indicate a J_c criteria of 15 Acm^{-2} for $\mu_0 H_{\text{irr}}$. (c) A comparison of the F_p between $\text{FeSe}_{1-x}\text{Te}_x$ and Co-doped Ba-122 ($T_c = 23.1 \text{ K}$) at reduced temperatures of $t = 0.68$ and 0.78 for $H \parallel c$ and (d) $H \perp c$. The data of Co-doped Ba-122 plotted as lines are taken from the Ref.¹³.

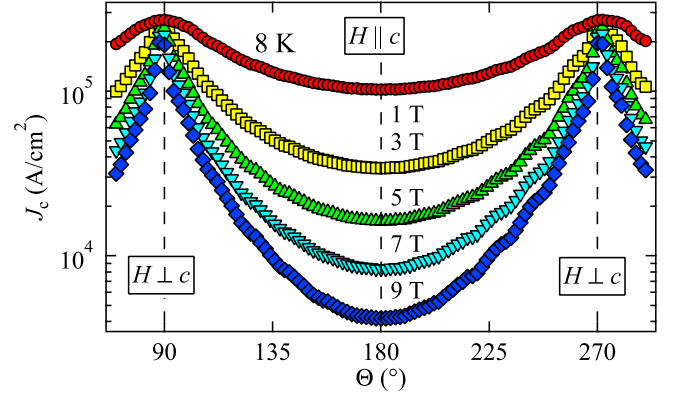


FIG. 5. (Color online) $J_c(\Theta)$ of the $\text{FeSe}_{1-x}\text{Te}_x$ film measured in several magnetic fields at 8 K. No additional peaks except at $H \perp c$ are observed.

by TEM in future.

The angular-dependent critical current densities ($J_c(\Theta)$) at 8 K in several magnetic fields, fig. 5, always show a peak positioned at $\Theta = 90^\circ$ and 270° owing to the intrinsic pinning.¹⁸ Here the magnetic field was applied in the maximum Lorentz force configuration ($H \perp J$) at an angle Θ measured from the c -axis. A small J_c anisotropy ($\gamma_J = J_c(90^\circ)/J_c(180^\circ)$) of 2.6 is observed at 1 T. This γ_J is significantly increasing with H (e.g. $\gamma_J = 46.8$ at $\mu_0 H = 9 \text{ T}$) due to the relatively close to H_{irr} in the c

direction.

In summary, epitaxial $\text{FeSe}_{1-x}\text{Te}_x$ films with sharp out-of-plane and in-plane texture have been realized on Fe-buffered single crystalline MgO substrates similar to the Fe/Ba-122 bilayers. These results indicate that Fe can work as generic buffer layer for epitaxial growth of Fe-based superconductors. The Fe/ $\text{FeSe}_{1-x}\text{Te}_x$ bilayer with a high T_c of 17.7 K showed strong intrinsic pinning from correlated *ab*-planes, since the Se(Te)-Se(Te) inter-layer distance is almost identical to the out-of-plane coherence length at low temperatures.

ACKNOWLEDGMENTS

The authors thank J. Scheiter and E. Reich for help with FIB cut samples and TEM, and E. Barbara for help with the AFM observation. We are also grateful to M. Kühnel and U. Besold for their technical support and S. Fähler for his RHEED software. This work was partially supported by DFG under Project no. BE 1749/13 and HA 5934/3-1. We also acknowledge the EU (IRON-SEA and SUPERIRON) under Project no. FP7-283141 and FP7-283204. S. W. acknowledges support by DFG under the Emmy-Noether program (Grant no. WU595/3-1).

¹M. J. Wang, J. Y. Luo, T. W. Huang, H. H. Chang, T. K. Chen, F. C. Hsu, C. T. Wu, P. M. Wu, A. M. Chang, and M. K. Wu, Phys. Rev. Lett. **103**, 117002 (2009).

²W. Si, Z. Lin, Q. Jie, W. Yin, J. Zhou, G. Gu, P. D. Johnson, and Q. Li, Appl. Phys. Lett. **95**, 052504 (2009).

³E. Bellingeri, R. Buzio, A. Gerbi, D. Marré, S. Congiu, M. R. Cimberle, M. Tropeano, A. S. Siri, A. Palenzona, and C. Ferdeghini, Supercond. Sci. Technol. **22**, 105007 (2009).

⁴P. Mele, K. Matsumoto, Y. Haruyama, M. Mukaida, Y. Yoshida,

Y. Ichino, T. Kiss, and A. Ichinose, Supercond. Sci. Technol. **23**, 052001 (2010).

⁵S. X. Huang, C. L. Chien, V. Thampy, and C. Broholm, Phys. Rev. Lett. **104**, 217002 (2010).

⁶S. Agatsuma, T. Yamagishi, S. Takeda, and M. Naito, Physica C **470**, 1468 (2010).

⁷E. Bellingeri, I. Pallecchi, R. Buzio, A. Gerbi, D. Marré, M. R. Cimberle, M. Tropeano, M. Putti, A. Palenzona, and C. Ferdeghini, Appl. Phys. Lett. **96**, 102512 (2010).

⁸Y. Han, W. Y. Li, L. X. Cao, X. Y. Wang, B. Xu, B. R. Zhao, Y. Q. Guo, and J. L. Yang, Phys. Rev. Lett. **104**, 017003 (2010).

⁹Y. Imai, T. Akiike, M. Hanawa, I. Tsukada, A. Ichinose, A. Maeda, T. Hikage, T. Kawaguchi, and H. Ikuta, Applied Phys. Express **3**, 043102 (2010).

¹⁰M. Hanawa, A. Ichinose, S. Komiya, I. Tsukada, T. Akiike, Y. Imai, T. Hikage, T. Kawaguchi, H. Ikuta, and A. Maeda, Jap. J. Appl. Phys. **50**, 053101 (2011).

¹¹I. Tsukada, M. Hanawa, T. Akiike, F. Nabeshima, Y. Imai, A. Ichinose, S. Komiya, T. Hikage, T. Kawaguchi, H. Ikuta, and A. Maeda, Appl. Phys. Express **4**, 053101 (2011).

¹²T. Thersleff, K. Iida, S. Haindl, M. Kidszun, D. Pohl, A. Hartmann, F. Kurth, J. Hänisch, R. Hühne, B. Rellinghaus, L. Schultz, and B. Holzapfel, Appl. Phys. Lett. **97**, 022506 (2010).

¹³K. Iida, S. Haindl, T. Thersleff, J. Hänisch, F. Kurth, M. Kidszun, R. Hühne, I. Mönch, L. Schultz, B. Holzapfel, and R. Heller, Appl. Phys. Lett. **97**, 172507 (2010).

¹⁴M. Schulze, M. Hacisalihoglu, C. Blum, C. Hess, M. Kumar, A. Wolter, S. Wurmehl, and B. Büchner, "Systematic investigations of the ternary system Fe-Te-Se (abstract, TT 10.28)," (2011), 75th Annual Meetings of the DPG and DFG Spring Meeting, Dresden, Germany.

¹⁵E. J. Kramer, J. Appl. Phys. **44**, 1360 (1973).

¹⁶M. Kidszun, S. Haindl, T. Thersleff, J. Hänisch, A. Kauffmann, K. Iida, J. Freudenberger, L. Schultz, and B. Holzapfel, Phys. Rev. Lett. **106**, 137001 (2011).

¹⁷C. Uher, J. L. Cohn, and I. K. Schuller, Phys. Rev. B **34**, 4906 (1986).

¹⁸M. Eisterer, R. Raunicher, H. W. Weber, E. Bellingeri, M. R. Cimberle, I. Pallecchi, M. Putti, and C. Ferdeghini, Supercond. Sci. Technol. **24**, 065016 (2011).